A measurement of the FP12 moderator brightness at LANSCE

Pil-Neyo Seo

May 11, 2003

1. Introduction

The NPDGamma collaboration has been constructing a beam line, flight path 12 (FP12), and the experiment at LANSCE to measure the gamma-ray asymmetry in the reaction of $\vec{n}+p\rightarrow d+\gamma$. The asymmetry is expected to be very small, 5×10^{-8}. A goal is to measure the asymmetry with 10% uncertainty [1]. The final size of the statistical error bar of the result will be determined by the neutron flux at the end of the neutron guide. In a spallation neutron source the neutron flux depends upon the proton current and its energy on the spallation target, moderator performance (brightness), neutron guide performance, and matter with which the neutrons interact before reaching the hydrogen target.

Flight path 12 views the new upper-tier cold hydrogen moderator. The performance of this moderator has not been experimentally studied but has been extensively modeled [2]. Knowledge of the moderator brightness is very important for the NPDGamma experiment because it gives the statistical limit that the experiment can achieve. There is also general interest to verify the spallation target models. These were the main reasons why the NPDGamma collaboration decided to measure the FP12 moderator brightness. In addition, this experiment allowed for the study the neutron guide performance.

The unique upstream/back-scattering moderator viewed by FP12 is a partially-coupled cold hydrogen (LH_2) moderator operated in supercritical state [3]. The measurement took place from Jan-9, 2003 to Jan-14, 2003. During the experiment the ortho-para ratio of hydrogen in the moderator was estimated to be about 23/77 [4]. Goals of the experiment were 1) to measure the FP12 moderator brightness, 2) to study the neutron guide performance, and 3) to verify the guide alignment.

The following people participated in the measurement; J.D. Bowman[1], M. Gericke[1], G. Greene[2], J. Long[3], G. Mitchell[1], S. Penttila[1], G. Peralta[1], P.-N. Seo[1], and W.S. Wilburn[1]

[1] P-23, LANL
[2] University of Tennessee/Oak Ridge National Laboratory
[3] LANSCE-3, LANL

The moderator brightness is a measure of the neutron phase space density on the moderator surface. In this work the brightness is given as the unit of neutrons/s/cm^2/sr/meV/µA, which includes corrections for the number of proton pulses per second, area on the moderator, a solid angle of the detector, an energy range of interest, and an average proton current. To measure the moderator brightness, we have to detect neutrons directly from the moderator, not neutrons that are reflected by the guide surface. To measure such direct neutrons, a two-pinhole collimator system was constructed and the second pinhole defines an active detector area. The two pinholes define the area viewed on the moderator surface as well as the solid angle of the detector. The pinhole collimators have to be fabricated from material that absorbs neutrons that are reflected from the guide surface because they are not aligned with the pinholes. The size of the pinholes also defines the neutron rate on the detector, which has to be limited to a level where the detector dead time will not be significant.

The neutron guide performance and its alignment were studied with the two-pinhole system by mounting the downstream pinhole and a detector on a scanner that could be moved on the x- and y- axes when the z-axis is along the beam.

In this technical note we describe the experimental setup, electronics, moderator brightness measurement, then data analysis and results, and we will discuss the neutron guide performance.

2. Experimental setup

2.1. LANSCE short-pulse spallation neutron source

The 625-μs long, 800-MeV H^- beam pulses from the LANSCE linear accelerator are injected into the Proton Storage Ring (PSR). As a part of the injection process, the H^- particles are stripped to H^+. In the PSR protons are accumulated and compressed into pulses with a roughly triangular-shaped longitudinal profile, 250-ns width at the base. The proton pulses are directed onto a spallation target at the rate of 20 Hz. During the experiment the average proton current was about 120 μA.

The spallation target consists of two 10-cm diameter tungsten cylinders. The upper cylinder is 7.5 cm long, while the lower cylinder is 27 cm long. The gap between cylinders is 14 cm and is surrounded by the four lower-tier moderators and reflector materials. FP12 views the upper-tier LH_2 moderator, which is above the upper tungsten cylinder in the back-scattered geometry. The active area of the moderator viewed by FP12 has the 12×12 cm^2 surface area.

2.2. Setup for the brightness measurement

Figure 1 shows the schematic top view of the experimental layout of the measurement (not to scale). The spallation target-moderator system is located in the target crypt, which is surrounded by a 5-m thick biological shield. The 7.93 m long neutron guide system, which starts at 1.37 m from the surface of the moderator, has a common vacuum housing, which during the experiment was filled with natural ^{4}He gas at the ambient pressure. The experimental apparatus was installed into a shielding structure in ER2. The length of the neutron flight path, from the moderator surface to the detector was 14.5 m.

The target crypt was kept under vacuum (about 0.3 Torr) and about 25% of the residual pressure was due to natural helium. Neutrons from the moderator enter the neutron guide through a 3.175-mm thick Aluminum window. The *m*=3 supper mirror guide system consists of the in-pile guide, the shutter guide, and the section of guide

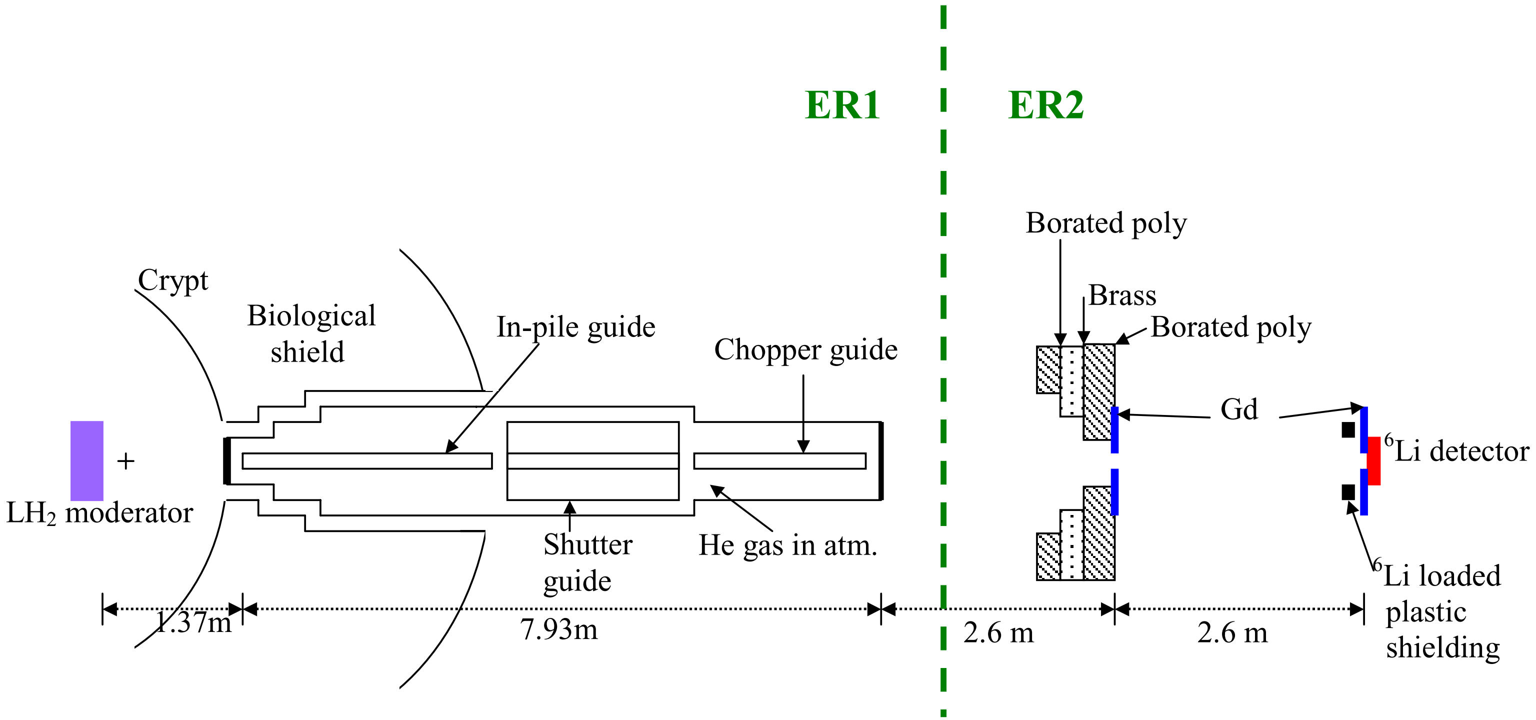

Figure 1. This is the layout of the beam line and experiment of the FP12 moderator brightness measurement (not to scale). Thickness of entrance/exit aluminum window of the guide envelope is 3.175/1.0 mm. The neutron guide was kept under natural He gas. The target crypt was under vacuum of 0.3 Torr and about 25% of the residual pressure in the target crypt is due to helium.

after the shutter. A detailed discussion of the neutron guide is in Section 4.

The neutrons leaving the guide pass through the exit window of 1 mm thick aluminum. Next they are collimated by the upstream gadolinium (Gd) pinhole. This pinhole was aligned to 1mm accuracy with respect to the center of the guide. After the upstream pinhole the neutrons traveled in air 2.6 m and were then collimated by a 2.3 mm thick ^{6}Li-loaded plastic that had a 3 mm diameter hole. The purpose of the ^{6}Li plastic was to absorb the neutrons without creating a gamma-ray background. Behind the ^{6}Li collimator was located the downstream Gd pinhole. Both of the Gd pinholes were 0.5-mm thick and 1.95±0.01 mm diameter. The ^{6}Li loaded plastic shield, the downstream Gd pinhole and the neutron detector with a photomultiplier tube (PMT, Phillips XP-2262/B) were mounted on a scanner that could be moved in the x and y axes.

The neutron detector was a ^{6}Li loaded glass scintillator that was 4 mm in diameter and 2 mm thick (Bicron Type NE905). This detector type has 6.6% of lithium by weight, which was 95% enriched ^{6}Li [5]. The density of the glass is approximately 2.2 g/cm^3. Since incoming neutron has a small kinetic energy the products from the reaction, α and ^{3}H, are emitted to the opposite direction in order to conserve the momentum. Ionization processes was caused by the 2.0-MeV alpha and 2.7-MeV triton from the reaction of ^{6}Li(n,α)^{3}H. The alpha and triton have ranges in glass about 7 μm and 40 μm, respectively [6]. As a result of de-excitation, fluorescent photons are emitted and detected by a PMT that generates an electrical pulse proportional to deposited energy in the ionization. The scintillator glass was doped with a small amount of cerium atoms. These impurity atoms speed up the de-excitation processes and thus increase the pulse height of the PMT. In silicate glasses, cerium is the only activator that produces fast scintillation light output useful for pulse mode operation [6].

2.3 Electronics for neutron counting

For the counting of the neutrons and to monitor the average proton current for normalization, NIM electronics were set up as shown in figure 2. Two signals were connected into the input of the electronics: one was from the PMT and the other was the average proton beam current from the accelerator.

The photons emitted as a result of the de-excitation in the ionization process in the scintillator glass were converted to an electric signal in the photocathode of the PMT. The PMT was operated at –1500 V. The PMT output was fed to the timing filter amplifier for pulse shaping. Then the signal was discriminated at a threshold, which was carefully set so that most of the neutrons were detected but not the gamma rays. The pulses from the discriminator went into a coincidence unit.

A signal, T_0, from a pickup coil in the accelerator, was used as a timing signal of a proton pulse hitting the tungsten target. The T_0 signal was available for the experiment through a "Lujan Timing Unit". Also, this unit provided a frequency signal, which was proportional to the average number of protons in the beam hitting the tungsten target. The Counter 2 in Fig. 2 was used to monitor the proton current.

Figure 3 illustrates some of the timing used in the setup. The time-of-flight (TOF) window, Δt, was selected to be less than 5% of the neutron TOF at each energy point. Time-of-flight of a 1 meV neutron in the 14.5 m long flight path is about 33 ms. Whenever neutron signals from the discriminator fall into the time window, the coincidence unit generated logic signals that were counted by Counter 1 in figure 2. Four signals were monitored during data acquisition: the T_0 signal, the gate signal, the discriminator output, and the coincidence signal as shown in figure 3. The T_0 signal triggered the gate with the width of Δt and with the delay of t.

A ^{6}Li-loaded glass scintillator is a well-known neutron detector. Figure 4 [5] shows pulse-height spectrum for neutron and gamma rays taken with a 1-mm thick ^{6}Li glass scintillator (type GS20 NE905). This is the same type as the one we used in this measurement. This detector has 6.6% total lithium and enriched to 95% ^{6}Li. According to this figure, gamma rays from a ^{60}Co source are in a continuous pulse-height spectrum that is smaller than neutron pulse height and the thermal neutron signature is peaked. To avoid the gamma-ray background the discriminator threshold has to be set. In order to find the optimized threshold, we scanned the discriminator threshold.

Figure 5 shows the number of counts as a function of the discriminator threshold. The blue curve presents the total number of counts (neutron and gamma ray counts). The red curve shows the gamma-ray contribution. Both were taken for same counting time and same electronic setup. This curve was obtained from measurement by covering the upstream pinhole with a Gd foil, which is an effective neutron absorber. The foil also produced gamma rays from the Gd(n,3γ) reaction, but because of the small solid angle this contribution to the gamma-ray background was insignificant. According to figure 5, the pulse height of the gamma rays varies and is significantly smaller than the neutron pulse height, thus allowing the use of the pulse-height discrimination. The discriminator threshold level was set to 250 mV and this level gave 4 kHz neutron count rate at 5-meV neutron energy as indicated in Table 1.

Figure 6 shows a typical waveform of a neutron pulse at the Timing Amplifier output. The signal returns back to the base line level at around 1 microsecond. This signal was fed into the discriminator and events above the threshold were sent to the coincidence unit. The discriminator pulse width of 800 ns determined the dead time of electronics. Given the peak event rate of 8.9 kHz at 15 meV, this indicates that the count loss due to the dead time is about 0.7%, which is a negligibly small error in this measurement. Signals only above the threshold (250 mV) were taken and the rest of parts were ignored and it was assumed that the electronics were 100% efficient.

3. Data Analysis and FP12 Moderator Brightness

Using the electronics described above, raw time-of-flight data were taken. The measurements were done in the neutron energy range of 0.8 meV to 80.9 meV. The background contribution was 0.7 % at 80.9 meV and 62% at 0.8 meV. Counting statistics

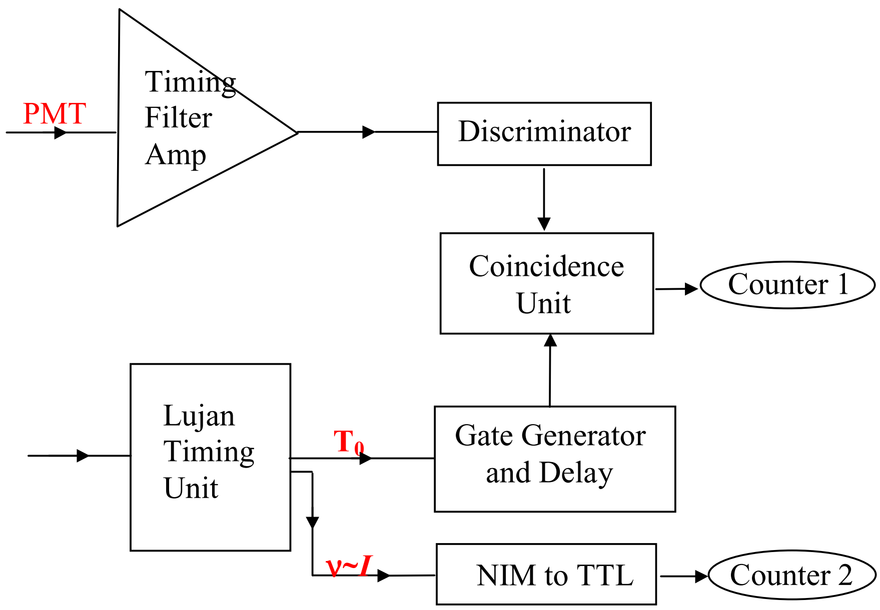

Figure 2. Logic diagram of the counting electronics. Counter 1 gives a number of neutrons in a delayed, *t* and TOF gate width, *Δt*. Counter 2 gives an average proton beam current. Counter 1 was gated by Counter 2.

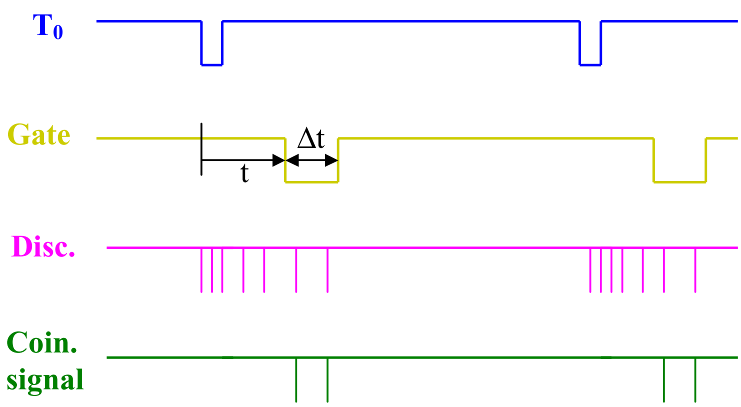

Figure 3. Four signals were monitored throughout the measurement. The proton trigger signal, T_o, comes every 50 ms. This signal triggered the gate, which was set for the delay (*t*) and time window (*Δt*) to select neutron energies of interest. Also, discriminator signals corresponding to detected neutrons were monitored. Neutrons arriving within the time window generated pulses from the coincidence unit.

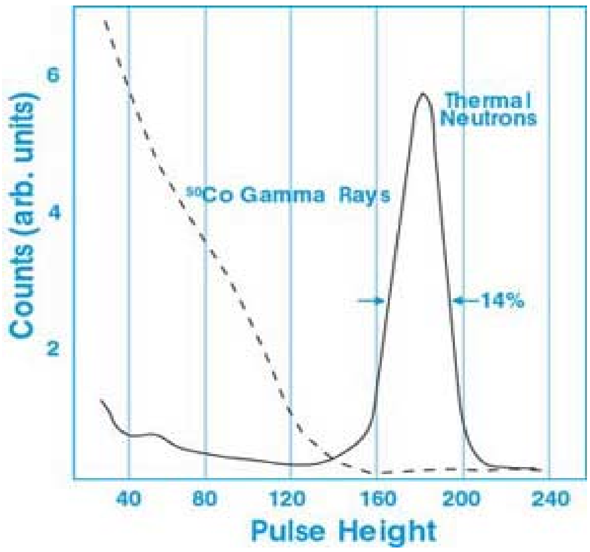

Figure 4. Pulse height spectra of gamma ray and neutron were taken with a 1-mm thick ^{6}Li glass scintillation detector, type GS20 NE905.

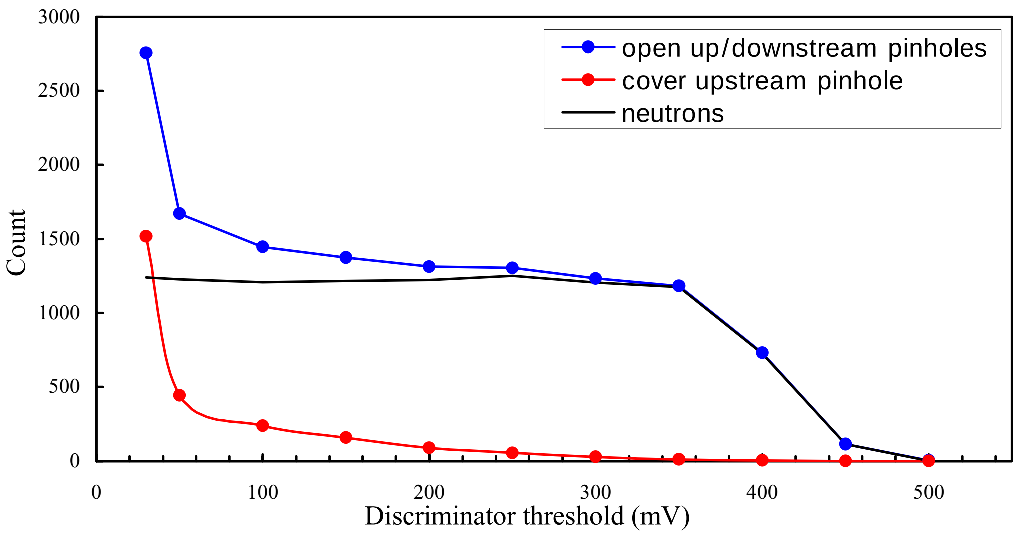

Figure 5. The ^{6}Li detector is sensitive to neutrons and gamma rays. To determine the pulse heights of neutrons and gamma rays, a number of counts were measured through the pinholes as a function of the discriminator threshold level (blue circle). Then the gamma-ray contribution was determined by mounting a neutron absorber, a Gd foil, onto the upstream pinhole (red circle). The solid black curve is background-subtracted neutron counts. Throughout the brightness measurement, the discriminator threshold level was set to 250 mV, which discriminated most of the gamma rays.

threshold	w/o Gd Rate	w/ Gd Rate	difference Rate
(mV)	(kHz)	(kHz)	(kHz)
500	0.01	0.00	0.01
450	0.36	0.00	0.35
400	2.28	0.01	2.27
350	3.70	0.03	3.67
300	3.85	0.09	3.77
250	4.08	0.17	3.90
200	4.10	0.28	3.82
150	4.29	0.49	3.80
100	4.52	0.74	3.77
50	5.22	1.39	3.83
30	8.62	4.74	3.87

Table 1. These are numerical values of the points shown in figure 4. The count rate at the threshold of 250 mV was about 4 kHz at 5 meV.

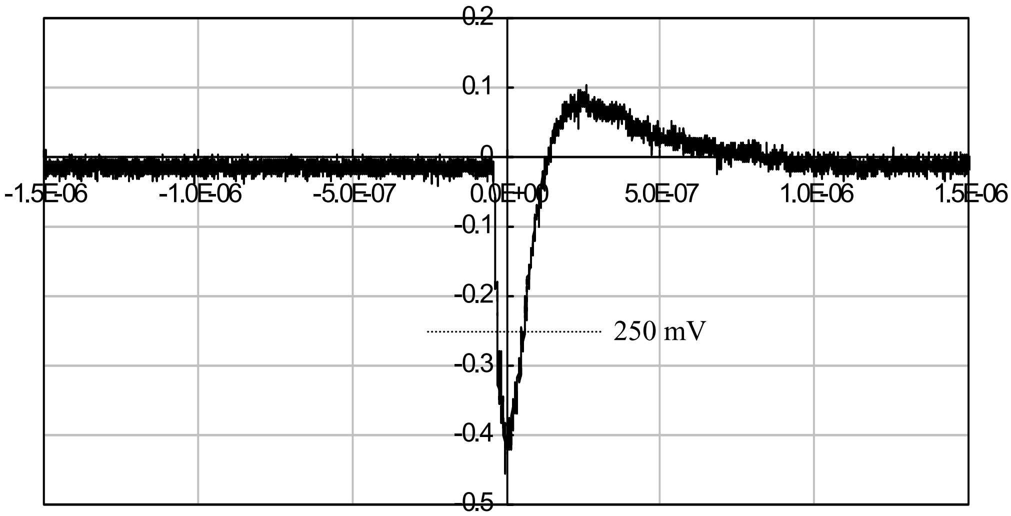

Figure 6. A typical waveform of a neutron pulse in the output of the Timing Filter Amplifier plotted as voltage (V) vs. time (μs). The discriminator threshold level of 250mV is indicated.

of 1.5 % at 80.9 meV and 4.6 % at 0.8 meV were achieved. Figure 7 shows a neutron TOF spectrum measured with the open up/downstream pinholes and a background spectrum measured with the upstream pinhole covered with the Gd foil.

The center of neutron peak in the time-of-flight spectrum is at 14.6 ms, which corresponds to the neutron energy of 5 meV as shown in the time spectrum. The maximum neutron rate is at about 3.3 meV as shown in the energy spectrum in figure 7. The peak represents the Maxwell-Boltzman distribution of the neutron velocities after moderation. The shape of the peak and its location depend upon weakly the Ortho/Para ratio of the hydrogen in the moderator.

The moderator brightness was calculated using the following formula:

$$B = \frac{n}{\text{activetime(ms/pulse)}} \times \frac{\Delta t(\text{ms})}{\Delta E(\text{meV})} \times 20\text{pulses/s} \times \frac{1}{\text{protoncurrent}(\mu\text{A})} \times \frac{1}{\Omega A(\text{cm}^2\text{sr})}$$

Here *n* is normalized and background-subtracted neutron counts. *Active time* is the total time used to count neutrons within the time window, i.e. a number of proton pulses times the width of the time window. The time dispersion for 14.5-m flight path is calculated by $\Delta t/\Delta E \equiv t/2E$. And ΩA is the product of solid angle, Ω, of the detector from the surface of the moderator, and *A,* the area on the moderator viewed by the detector.

Two sets of data were taken and analyzed to obtain the FP12 moderator brightness. One data set was measured using the pinholes made of ^{6}Li plastics and the other data set was measured using the pinholes made of the Gd foil. The measurement with the Gd pinholes has better statistics.

Each step in the data analysis for using the Gd foil as an example is listed in Table 2. Neutron energy, *E*, was calculated using the TOF (TOF= *t*, delay (ms)) and the 14.5 m length of the flight path. Counts in columns Neutron and Background are a number of neutrons (*N*) in the time width (Δt, gate width (ms)) when the up/downstream pinholes were open and a number of background counts (*B*) when the upstream pinhole was covered. Corresponding proton currents are given in the columns Proton (P_N) and Proton (P_B) are given for *N* and *B* respectively. To normalize the counts, the ratio of the proton currents were formed and then multiplied with the background counts (*B*) and subtracted from the neutron counts (*N*). Count time gives the run time of the measurement. T_0 gives the number of total proton pulses during count time. *Active time* is give by the product of the gate width and the number of pulses. *Rate (tof)* gives the instantaneous neutron rate per pulse per ms. The rate as a function of TOF is shown in figure 7 (top).

Rate (tof), n/ms/T_0, is multiplied by time dispersion (column $\Delta t/\Delta E$ in the second page of Table 2) to obtain a rate as a function of the neutron energy plotted in figure 7 (bottom). Since the proton pulse rate was 20Hz, the *Rate (energy)*, n/meV/T_0, was multiplied by 20Hz and this gives *Rate (second)*, /n/meV/s. This Rate was normalized by the proton beam current, 120μA given *Rate (proton)*, n/meV/s/μA. The next column, Uncorr_bright, was obtained by dividing the last Rate by the product of the area (*A*) viewed on the moderator surface (0.93 cm^2) and solid angle of the detector (Ω)(1.42×10^{-8} sr). This is uncorrected brightness data.

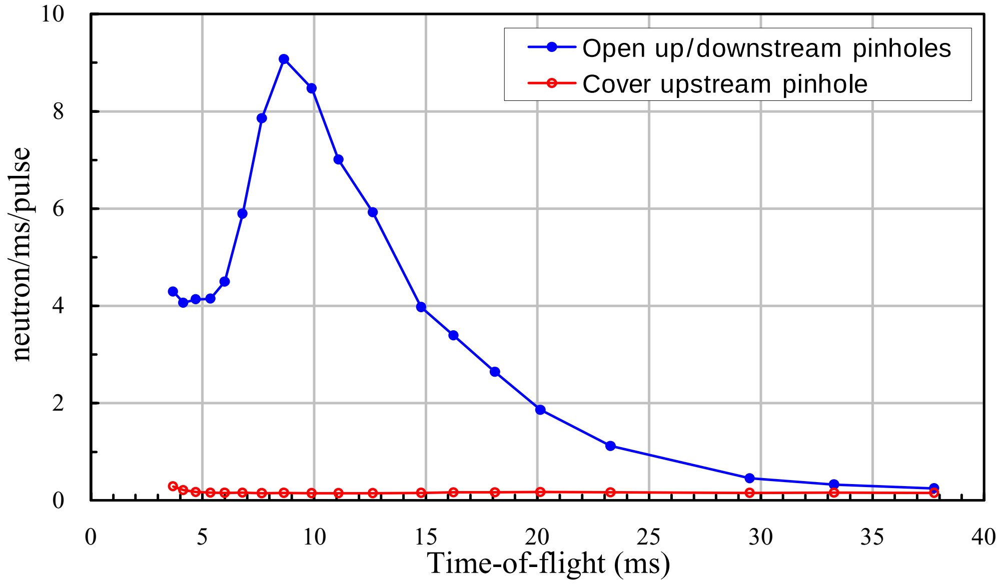

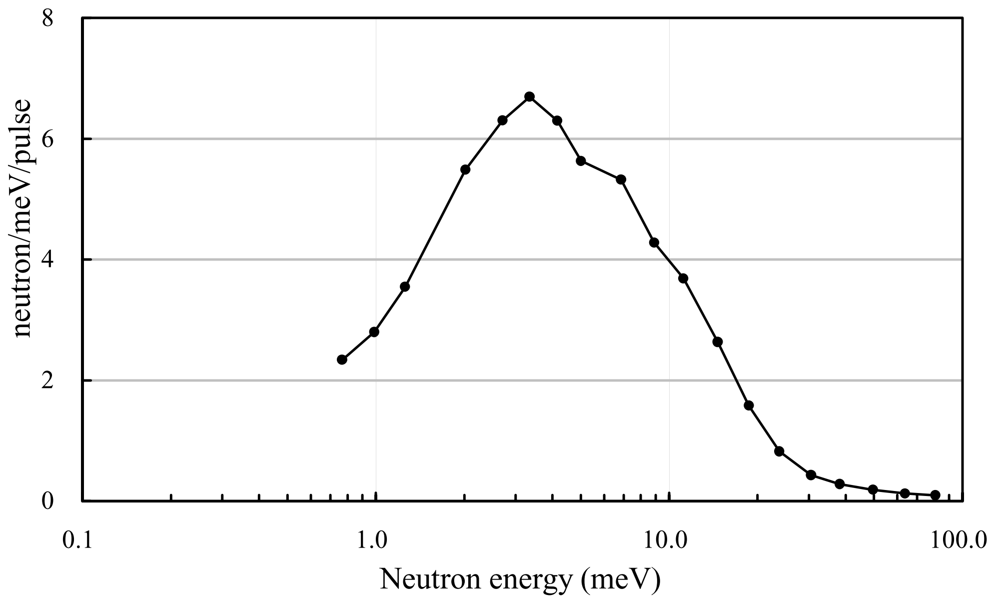

Figure 7. The top figure shows a neutron time-of-flight spectrum when the up/downstream pinholes were open (filled circle) and an energy spectrum when the upstream pinhole was covered by a Gd foil in order to define the gamma-ray background (open circle). The bottom figure gives a corresponding normalized neutron spectrum as a function of the neutron energy. The measurement covered the energy range from 80.9 meV to 0.8 meV.

E (meV)	Delay(t) (ms)	gate width/T_0 (ms)	Gd-out Proton(P_N)	Neutron (N)	Bkgd (B)	Gd-in Proton(P_B)	norm ratio (P_N/P_B)	Norm of B (P_N/P_B)*B	Norm of N N-(P_N/P_B)*B	Count time (s)	T_0 (pulses)	Active time (ms/T_0)
76.85	3.68	0.2008	17857480	5131	218	11342366	1.5744	343.220	4787.8	297.62	5952.49	1195.26
60.94	4.144	0.2009	18500729	5031	225	15892629	1.1641	261.924	4769.1	308.35	6166.91	1238.93
47.56	4.703	0.2009	18309645	5069	200	17586670	1.0411	208.222	4860.8	305.16	6103.22	1226.14
36.55	5.355	0.2497	14712319	5079	216	16504836	0.8914	192.541	4886.5	245.21	4904.11	1224.56
29.27	5.998	0.2496	13649192	5111	214	16461538	0.8292	177.440	4933.6	227.49	4549.73	1135.61
22.90	6.796	0.2495	10758670	5275	213	16089103	0.6687	142.432	5132.6	179.31	3586.22	894.76
17.58	7.658	0.5005	5677864	7442	502	20040000	0.2833	142.230	7299.8	94.63	1892.62	947.26
13.87	8.65	0.5004	3530887	5343	501	19751713	0.1788	89.561	5253.4	58.85	1176.96	588.95
10.64	9.9	0.5002	7345799	10376	502	20284920	0.3621	181.790	10194.2	122.43	2448.60	1224.79
8.52	11.102	0.5002	9163167	10700	503	20284920	0.4517	227.217	10472.8	152.72	3054.39	1527.81
6.61	12.637	0.5002	10252930	10132	501	20284920	0.5054	253.228	9878.8	170.88	3417.64	1709.51
4.85	14.788	0.5000	15350695	10157	1002	39481362	0.3888	389.586	9767.4	255.84	5116.90	2558.45
4.03	16.239	0.5000	18166188	10261	1004	36426340	0.4987	500.705	9760.3	302.77	6055.40	3027.70
3.26	18.095	0.5000	23077226	10154	1008	36931179	0.6249	629.870	9524.1	384.62	7692.41	3846.20
2.64	20.141	0.5000	16788793	5206	1030	36283788	0.4627	476.589	4729.4	279.81	5596.26	2798.13
1.98	23.277	0.5002	27987093	5226	1002	36180378	0.7735	775.090	4450.9	466.45	9329.03	4666.38
1.22	29.500	1.0020	33483997	5115	1513	29295792	1.1430	1729.303	3385.7	558.07	11161.33	11183.65
0.96	33.292	1.0020	46968368	5157	1018	18735531	2.5069	2552.039	2605.0	782.81	15656.12	15687.43
0.75	37.768	1.0020	63529408	5298	1085	21019997	3.0223	3279.230	2018.8	1058.82	21176.47	21218.82

Table 2. Brightness data are shown with different corrections. This is data using the Gd pinholes.

Rate(TOF) $n/ms/T_0$	$\tilde{t}/2E$ (ms/meV)	Rate(energy) $n/meV/T_0$	Rate(second) n/meV/s	Rate(proton) n/meV/s/uA	Uncorr_bright n/meV/s/uA/ cm^2/sr	(^{6}Li Detector Efficiency) × (Count loss)	Det_uncorr_bri n/meV/s/uA/ cm^2/sr	Al/air/He correction	Brightness	Error (count)	Uncertainty (brightness)
4.01	2.394E-02	0.096	1.918E+00	1.598E-02	1.212E+06	0.810	1.497E+06	0.814	1.839E+06	73.99	1.318E+05
3.85	3.400E-02	0.131	2.618E+00	2.181E-02	1.653E+06	0.844	1.960E+06	0.802	2.444E+06	72.75	1.751E+05
3.96	4.944E-02	0.196	3.920E+00	3.267E-02	2.476E+06	0.876	2.825E+06	0.799	3.536E+06	72.64	2.531E+05
3.99	7.325E-02	0.292	5.846E+00	4.872E-02	3.692E+06	0.906	4.077E+06	0.795	5.128E+06	72.61	3.669E+05
4.34	1.025E-01	0.445	8.902E+00	7.419E-02	5.623E+06	0.926	6.069E+06	0.792	7.663E+06	72.72	5.482E+05
5.74	1.484E-01	0.851	1.702E+01	1.418E-01	1.075E+07	0.945	1.138E+07	0.787	1.445E+07	73.60	1.033E+06
7.71	2.178E-01	1.679	3.358E+01	2.798E-01	2.121E+07	0.960	2.208E+07	0.781	2.828E+07	87.09	2.008E+06
8.92	3.119E-01	2.782	5.564E+01	4.636E-01	3.514E+07	0.970	3.622E+07	0.775	4.674E+07	73.71	3.337E+06
8.32	4.659E-01	3.878	7.755E+01	6.463E-01	4.898E+07	0.977	5.014E+07	0.767	6.537E+07	102.75	4.623E+06
6.85	6.519E-01	4.468	8.937E+01	7.447E-01	5.644E+07	0.980	5.760E+07	0.759	7.589E+07	104.53	5.366E+06
5.78	9.564E-01	5.527	1.105E+02	9.211E-01	6.982E+07	0.981	7.115E+07	0.749	9.500E+07	101.91	6.722E+06
3.82	1.524E+00	5.820	1.164E+02	9.700E-01	7.352E+07	0.981	7.497E+07	0.733	1.023E+08	102.70	7.239E+06
3.22	2.013E+00	6.489	1.298E+02	1.082E+00	8.197E+07	0.980	8.368E+07	0.723	1.157E+08	103.74	8.194E+06
2.48	2.777E+00	6.876	1.375E+02	1.146E+00	8.686E+07	0.978	8.882E+07	0.709	1.253E+08	103.85	8.875E+06
1.69	3.819E+00	6.455	1.291E+02	1.076E+00	8.154E+07	0.976	8.356E+07	0.693	1.206E+08	75.38	8.657E+06
0.95	5.876E+00	5.605	1.121E+02	9.341E-01	7.080E+07	0.972	7.281E+07	0.668	1.090E+08	77.47	7.862E+06
0.30	1.210E+01	3.664	7.328E+01	6.107E-01	4.629E+07	0.965	4.795E+07	0.618	7.758E+07	82.73	5.752E+06
0.17	1.733E+01	2.878	5.757E+01	4.797E-01	3.636E+07	0.961	3.782E+07	0.589	6.422E+07	87.80	4.989E+06
0.10	2.522E+01	2.400	4.799E+01	3.999E-01	3.031E+07	0.957	3.169E+07	0.556	5.700E+07	92.61	4.770E+06

solid angle*area:

solid angle:	1.420E-08
area:	0.929
Ω*area:	1.319E-08

Figure 8 shows how the product ΩA was derived. The detector at distance D_1+D_2 views the moderator through the upstream pinhole. The detector solid angle from the moderator is $\Omega=\pi s^2/(D_1+D_2)^2$. The area on the moderator, A, viewed by the detector is defined as $\pi r^2(D_1+D_2)^2/D_2^2$ where r is the radius of the upstream pinhole, D_1 and D_2 are distance from the surface of the moderator to the upstream pinhole and distance from the upstream pinhole to the detector. Neutrons from the area on the moderator, A, within the solid angle, Ω, are detected by the detector. This gives the brightness in the unit of neutrons/s/meV/cm^2/sr/μA.

Analyzed data were corrected for the efficiency of the ^{6}Li glass scintillation detector, the 4.175-mm thick Al window in the guide, the attenuation of natural He gas which was inside the guide and air between the exit window of the guide and the detector. The efficiency of the detector was obtained from the products of neutron absorption in the detection material and of collection efficiency. As described in section 1, this glass scintillator contains 6.6% Li by weight which is 95% ^{6}Li enriched evenly distributed over the detector volume. The neutron detector efficiency depends on the n-^{6}Li absorption cross section, σ, of the reaction ^{6}Li(n,α)t, and the density of the ^{6}Li, n, and the thickness of the detector, t. This cross section is well known to the accuracy less than 1% level and has the neutron energy dependence of σ=149/sqrt(E), where E is in eV and σ is in barn (10^{-24}cm^2) [8]. The detector efficiency can be written as,

$$\varepsilon = 1 - e^{-n\sigma t} = 1 - e^{-\frac{0.464}{\sqrt{E}}},$$

where E is in eV, n=0.1557×10^{23}/cm^3, and t=0.2 cm. The detection efficiency varies from 80.4% to 99.99% for the neutron energy from 80.9 meV to 0.8 meV. In addition to the detection efficiency, “edge effects” have to be considered. Near the detector surface where low energy neutrons are captured, one of reaction products can escape the detector, and the deposited energy by remained reaction product through ionization is below the threshold of pulse height in the discriminator unit. A Monte Carlo calculation showed that 3.8% and 0.6% of 1-meV and 100-meV neutrons are lost respectively through this process. The “edge effect” depends on the neutron energy and the distribution of ^{6}Li in the glass. In the calculation, it was assumed that ^{6}Li atoms were distributed uniformly in the detector material. The detector efficiency, ε, was corrected by this “edge effect”. The corrected detector efficiency is given in the column Detector Efficiency of Table 2 and shown in figure 9. The brightness, Uncorr_bright, was corrected by the detector efficiency and the result is given in column “Det_Uncor_bri”.

The next correction was the attenuation caused by the Al windows of the neutron guide. The entrance window was 3.175mm thick and the exit window 1.0mm. Total cross section of a solid aluminum is approximated to be the half of the total cross section of free aluminum atoms [9] in order to include the Bragg scattering of neutrons within energy range of 0.1meV- 82 eV. A correction for a solid Al was thus obtained by calculating transmission of the half of total Al thickness. In figure 10, the neutron transmission of a 4.175-mm thick free Al is compared to that of a 2.088-mm thick solid Al. In both cases, the Al attenuation contribution in the brightness is less than 10%.

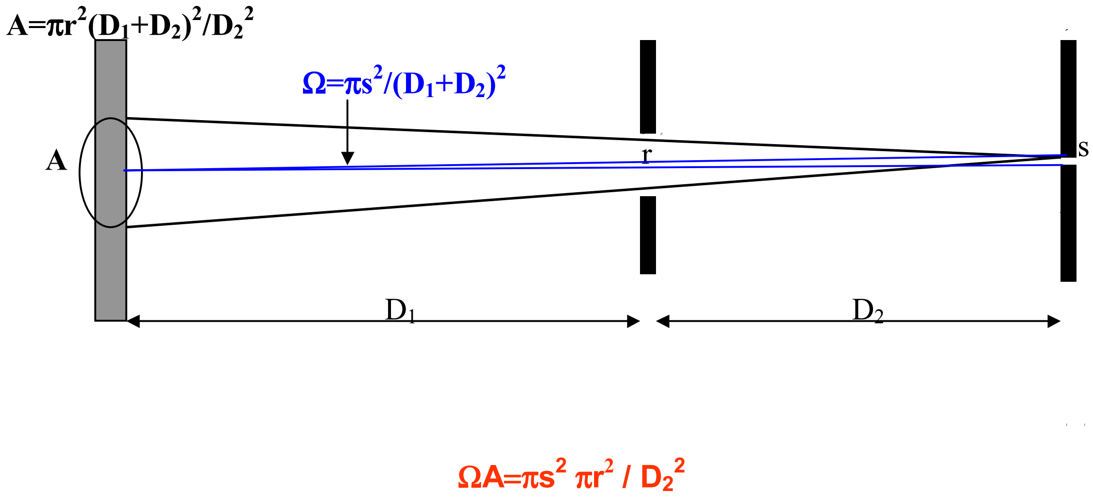

Figure 8. The moderator brightness measurement was done using two pinholes system. The solid angle, $\Omega=\pi s^2/(D_1+D_2)^2$, is the detector solid angle from the moderator. An area of the moderator surface, A, viewed by a point detector is $A=\pi r^2(D_1+D_2)^2/D_2^2$, the radii of up/downstream pinholes are r and s, respectively. The product of a detector solid angle detector and an area viewed on the moderator is, $\Omega A=\pi s^2\pi r^2/D_2^2$.

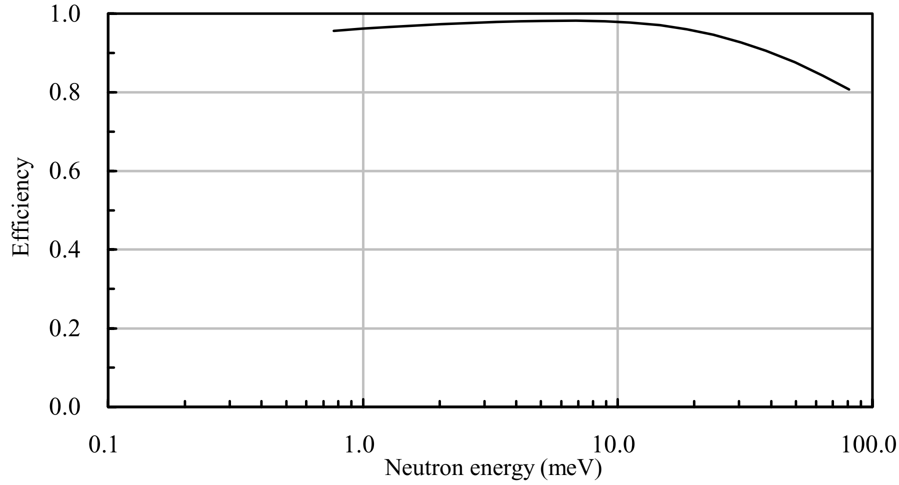

Figure 9. The neutron detection efficiency of the ^{6}Li glass scintillation detector is shown as a function of the neutron energy.

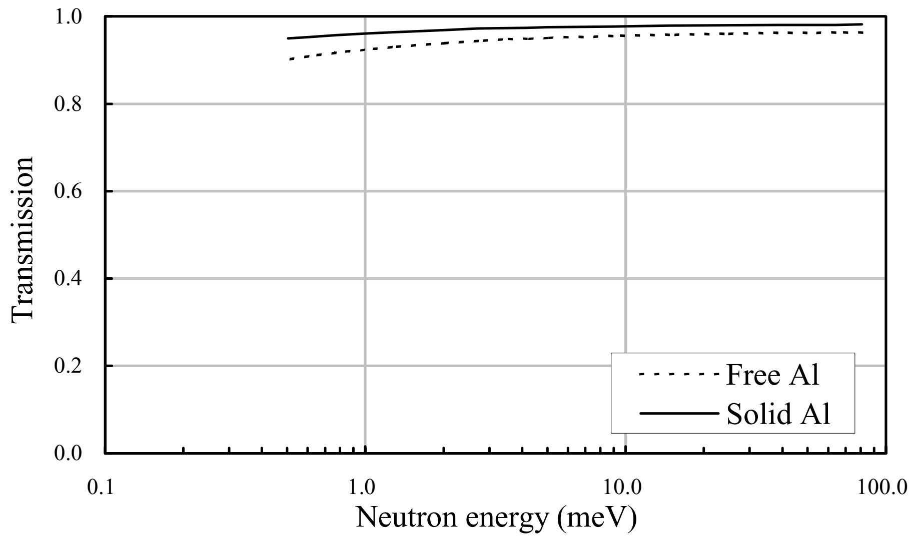

Figure. 10. Neutron transmission through Al using the free-Al cross section (solid) and the solid-Al cross section (dash), see text.

The 7.93-m long section of the neutron guide was filled with natural He gas to atmospheric pressure (about 580 Torr at Los Alamos) for cooling the source end of the guide. The brightness data has to be also corrected for the attenuation of this He gas. Natural He gas is composed of mostly ^{4}He and 1.37×10^{-6} of ^{3}He. Neutron absorption by ^{3}He was negligible because their fraction is very small although cross sections are high at low energies. The 7.93 m of ^{4}He scattered 1-5% of the neutrons in 0.8 to 80.9-meV energy range. Between the guide exit window and the detector was 5.2 m of air that also attenuated the beam; 75% of nitrogen and 25% of oxygen in air absorbed/scattered neutrons by 15-37% and by 2-4%, respectively. Most of scattering in air is due to nitrogen because nitrogen has higher cross section and higher fraction of composition. Total correction due to the aluminum windows, the He gas, and air ranges from 18.6% at 80.9meV to 44.1% at 0.8meV and are listed in Table 2 in column Al/air/He correction. The corrected brightness is given in column Brightness.

In figure 11, measured and corrected brightness is compared to Monte Carlo N Particle (MCNP) model-calculated brightness by LANSCE-12. In the measurement a 0.5-mm thick Gd collimator with a 1.95-mm diameter pinhole was placed in front of the detector. For the upstream collimation was used a 0.5-mm thick Gd with a 1.95mm diameter pinhole was in front of the upstream shielding as shown in figure 1. The result of this measurement is shown by blue points (filled circle). Another measurement with a worse statistics was done using a ^{6}Li loaded plastic sheet with an effective 1.93mm diameter pinhole in the front of the detector and a ^{6}Li loaded plastic with an effective 2mm diameter pinhole as an upstream collimation. The result of this measurement is shown in red (open square). For both measurements, the detector and a PMT was located at x=2.01mm and y=2.02mm from the nominal center of the flight path. The neutron counts were corrected as described above. Error bars of brightness were determined by statistical errors and systematic errors. Statistical errors are from 1.5 to 4.6 %. Largest contribution in 7 % systematic uncertainty came from the uncertainty in the proton beam current, 5 % and the uncertainty from electronics was negligible. Both measurements agree with each other. The brightness used in the NPDGamma proposal in 1997 based on the MCNP Physics model by LANSCE-12 [1,2]. LANSCE-12 has redone the MCNP As-built model calculation for the FP12 moderator recently [4]. Difference in the models is basically how much details were included. This explains the difference in brightness calculations (black line and dashed green). The measured maximum brightness of 1.25×10^8 n/s/cm^2/sr/meV/μA at 3.3 meV is a factor of 1.5 smaller than the value of the most recent calculation. Measured brightness is an average over the area, 0.929cm^2, on the center of the moderator, whereas calculated brightness is an average over the entire moderator area. This causes even bigger discrepancy, a factor of 2, between measured brightness and calculated brightness. We think that the discrepancy caused by 1) the modeling, 2) ortho/para-hydrogen ratio during measurement, 3) moderator non-uniformity, 4) a modeling code, and 5) estimation of systematic errors in measurement.

4. Study of the neutron guide performance and alignment

As described in previous sections, the FP12 guide is an *m*=3 supermirror (SM) guide. One of the goals of the experiment was to study the guide performance and its

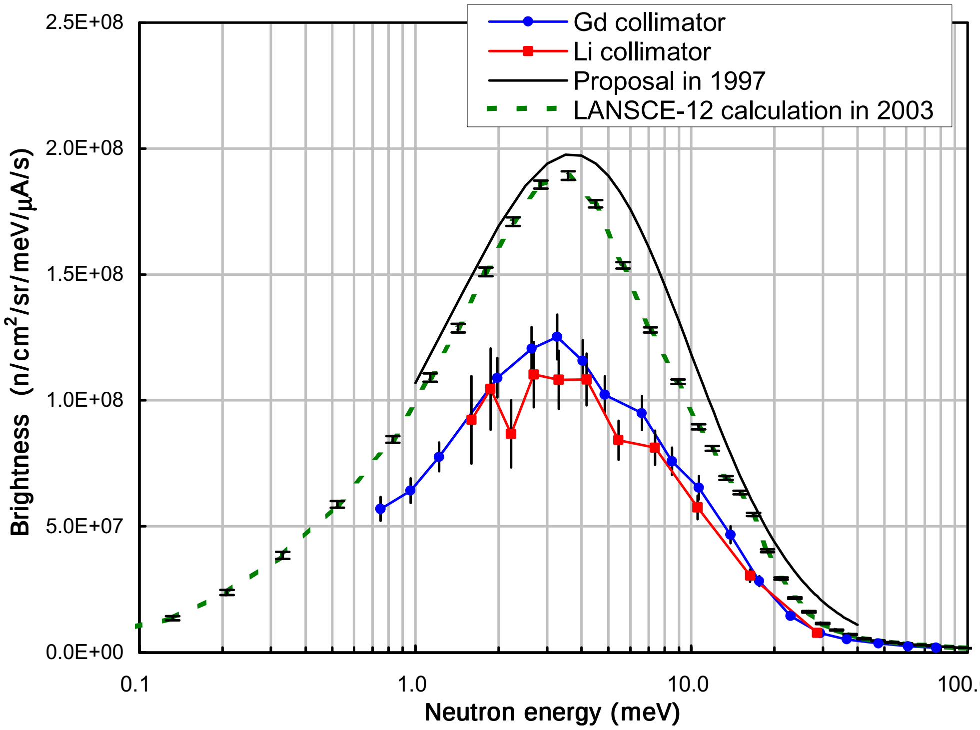

Figure 11. The measured FP12 brightness is compared to a MCNP model calculation. Blue dots show the result of the measurement where Gd foils with 1.95mm diameter pinholes at up/downstream. The red circles show the result of using ^{6}Li loaded plastic sheets with 1.93mm diameter pinholes at up/downstream. Measured brightness is averaged over the center area, 0.93cm^2, on the moderator. The black line and green dashed line show the predicted brightness, see text.

alignment. In order to do this, the detector and the downstream collimator shown in figure 1, was moved perpendicularly respect to the beam direction, in x- and y- direction, to view the guide.

The advantage of an m=3 SM guide is that the critical angle of total reflection is about three times that of conventional nickel guide and thus, more neutrons come out of the guide. However, neutron reflection losses are higher than those of single layer of nickel coatings [9,10]. Critical angle of Ni/Ti multiplayer is defined as $\theta_c = m \times \theta_c(^{nat}\mathrm{Ni})$ [11], where $\theta_c(^{nat}\mathrm{Ni})$ corresponds to the critical angle of a neutron with a perpendicular velocity of 7 m/s. A typical measured reflectivity curve of FP12 SM guide using 4.27-Å neutrons is shown in figure 12 as a function of the glancing angle $m = \theta_c / \theta_c(^{nat}\mathrm{Ni})$. The reflectivity at

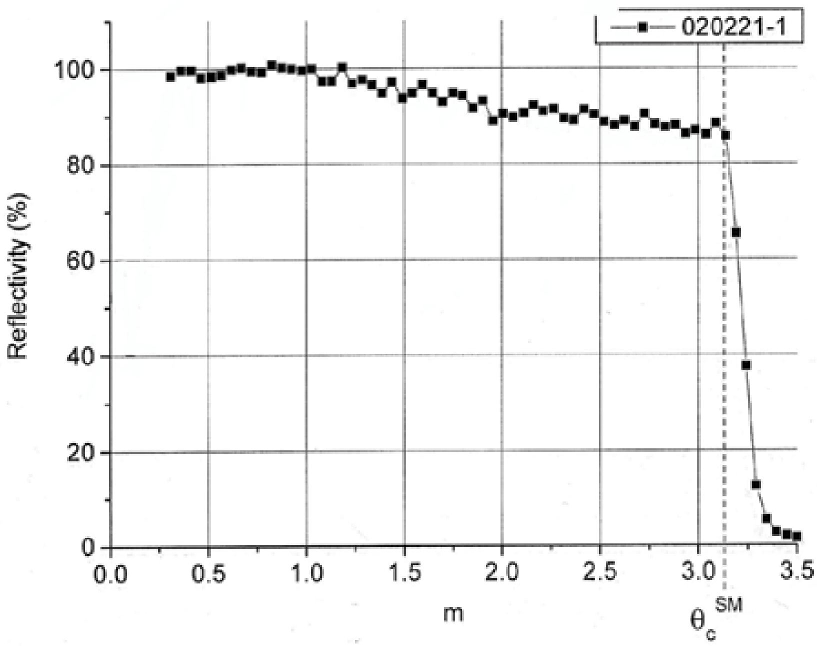

Figure 12. At m=3.13 reflectivity is 86.5% for λ=4.27-Å neutrons. Measured reflectivity of FP12 guide section.

m=3.13 is 85.6% for λ=4.27 Å. Critical angles for the neutron energy from 0.8 to 80.9 meV can be calculated by using the equation, $\theta_c = m\times\theta_c(^{nat}\mathrm{Ni})$, where m=3 and $\theta_c(^{nat}\mathrm{Ni}) = 1.73\times10^{-3}$ (λ/Å). Neutrons with perpendicular velocity less than 21m/s are reflected by the guide and neutrons with the perpendicular velocity >21m/s interact with atoms of Ni/Ti in layers rather than are bounced.

To study the guide performance and alignment, the detector was placed at the nominal center of the flight path and then, it was remotely moved by about 2-mm steps in x direction for the Left/Right (L/R) scan and in y direction for the Up/Down (U/D) scan. Neutron energy of 10 meV was selected by setting the TOF to 10-ms with 200-μs gate width for 400T_0's. Schematic diagram of this measurement is given in Fig. 13.

Direct and/or reflected neutrons pass the collimator of the radii of up/downstream indicated as "r" and "s" respectively and observed by the detector as shown in Fig. 13. The figure shows different neutron trajectories starting from the moderator, going into the guide, being reflected by the guide, passing the collimators and finally arriving at the detector. Possible neutron paths are indicated as "a, b, c, and d". Neutrons of the path "b" are going onto a detector directly from the moderator and neutrons with paths "a, c, and d" are reflected once or twice by the neutron guide. Neutrons in this guide system can have maximum of two bounces.

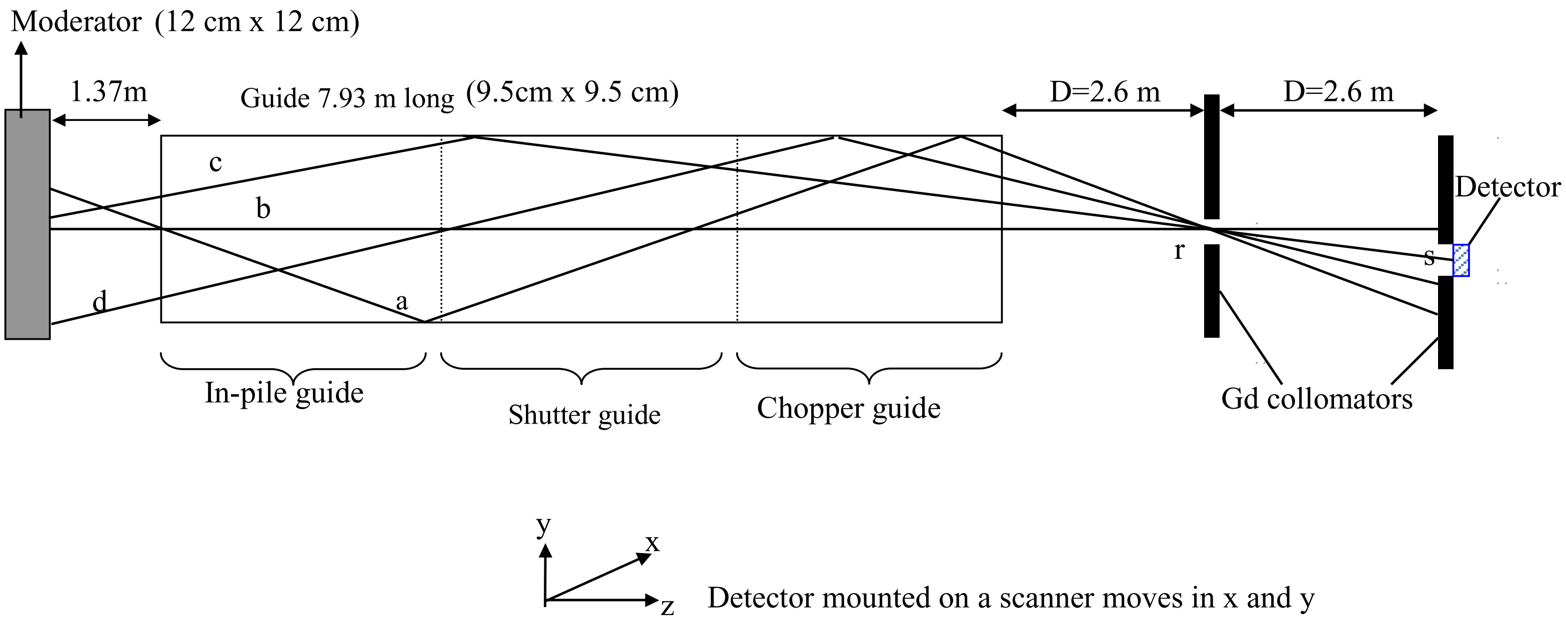

Figure 13. Different neutron paths from the moderator to the detector. Possible paths are labled as "a, b, c, and d" indicating reflected and no reflected neutrons. A neutron can have maximum of two total reflections in the guide system of this experiment.

The results of x and y scans are shown in Fig. 14. The R/L and U/D scan results show the similarity in general shape such as 1) no neutron was observed beyond approximately ±4 cm in x and y off the nominal center of the flight path because the detector sees the edge of the guide, 2) between 0~±1 cm of the detector location in x and y axes no bounced neutron was observed, 3) between ±1~±3 cm in both axis shows one bounced neutrons were observed, and 4) between ±3~±4 cm in both axis shows two bounced neutrons were observed. However, a small peak in –4~-5 cm in U/D scan was observed because the moderator was placed 1 cm offset vertically.

For the two-pinhole system used in this measurement, Monte Carlo simulation was done with the 10-meV neutron energy for the beam profile viewed by the detector as shown in Fig. 15. The Monte Carlo included the same geometry as the experimental setup. The moderator in the model has 1-cm offset in y axis. Its result shows that the structure in the neutron guide performance by the simulation looks as same as the measurement. The size of the beam is about ±4 cm in x and y axes, which was confirmed in measurement shown in Fig. 14. We also confirmed our interpretation of neutron bounce by the guide in the L/R and U/D scans from the Monte Carlo simulation. Simulation for number of reflection for 10-meV neutrons traveling down the guide through the downstream pinhole shows that most of neutrons were reflected at least once and the number of reflection is limited by twice. This also assures that the detector at the nominal center of the flight path viewed only direct neutrons from the moderator, which used in brightness.

5. Conclusion

The NPDGamma collaboration has measured the brightness of the FP12 upper-tier partially coupled cold hydrogen moderator. A two-pinhole system was used with a high efficient ^{6}Li glass scintillation detector. The brightness from the 0.93-cm^2 area on the moderator has a maximum of 1.25 n/s/sr/cm^2/meV/µA at 3.3 meV. Statistical uncertainty and systematic error were about 2 % and 7 % respectively. Compared this to the model calculation in the 1997 NPDGamma proposal, measurement is a factor of 2 lower than the prediction at the maximum brightness. The performance of the *m*=3 SM neutron guide was also studied by moving the detector with the downstream collimator in L/R and U/D axes. The result of this scanning shows that 1) the beam is in a square shape and flat in intensity, 2) zero-, once- and twice-reflected neutrons by the guide were observed, and 3) the moderator is positioned symmetric in x axis and about 1 cm offset in y axis respect to the nominal center of the flight path. A Monte Carlo simulation of neutron transportation through the guide confirmed our interpretations of the measurement results.

Reference:

[1] NPDGamm Proposal, http://p23/len/npdg/proposal/proposal.html.

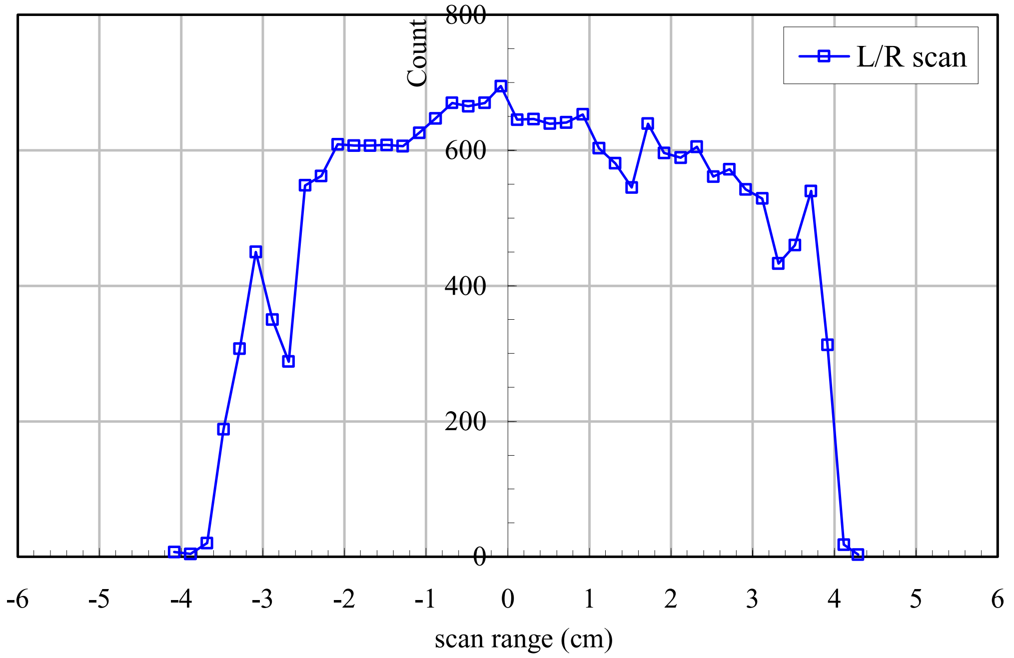

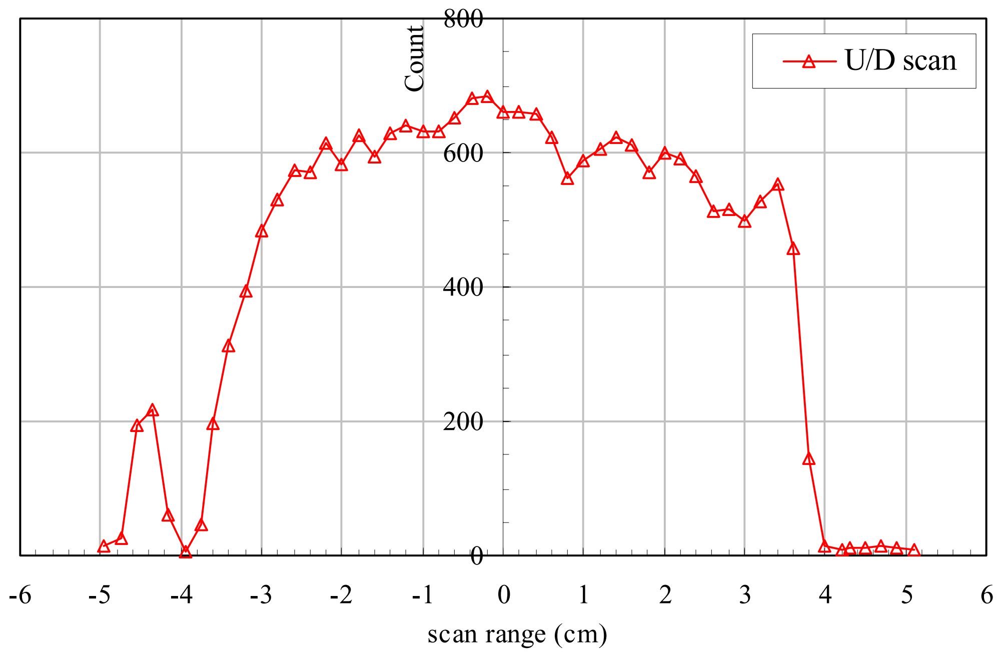

Figure 14. Results of the L/R and U/D detector scans with 10-meV neutrons.

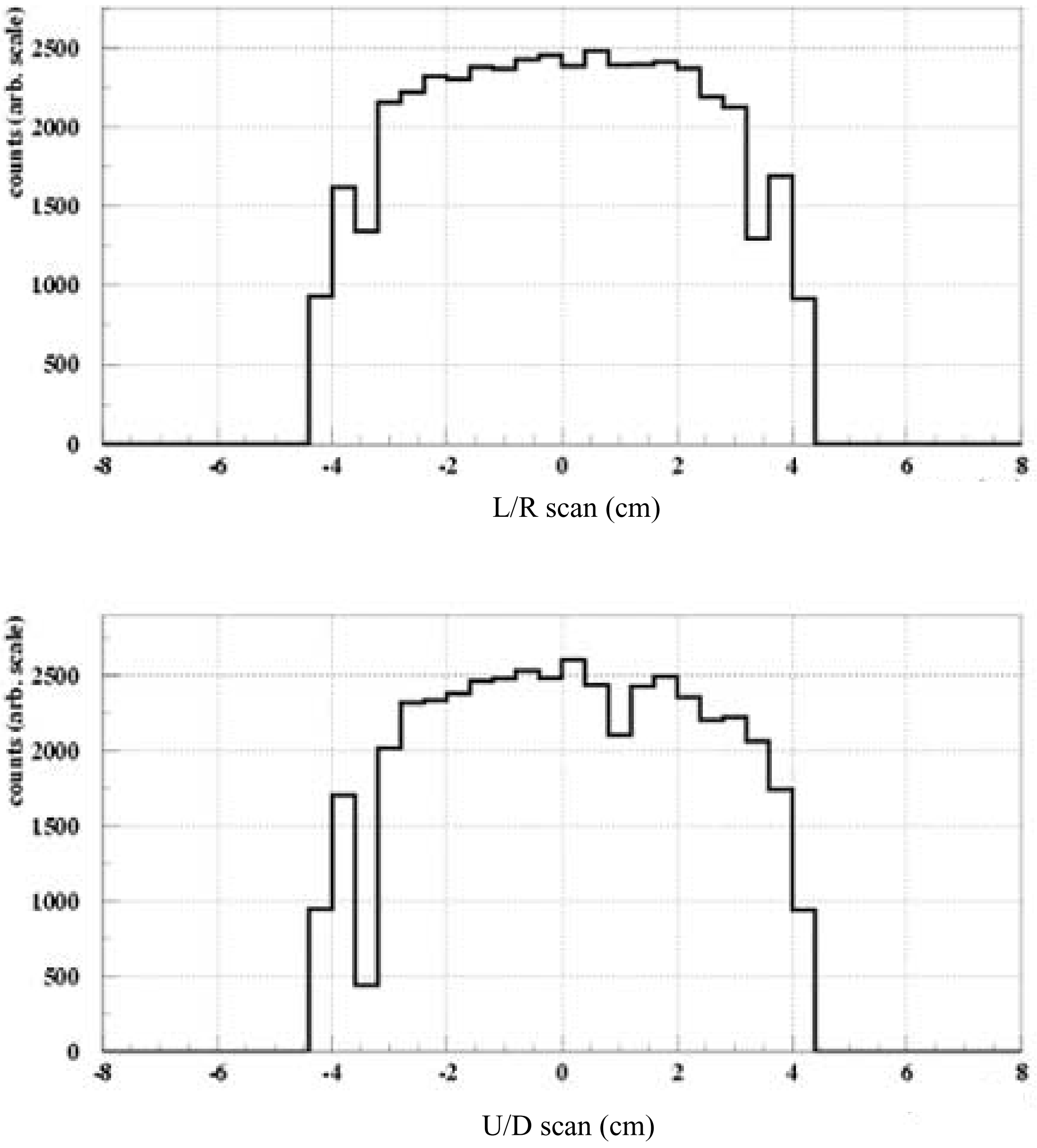

Figure 15. Monte Carlo generated beam profile in X and Y direction for 10-meV neutron energy for the experimental setup used in this measurement.

[2] G. Muhrer, P.D. Ferguson, G.J. Russell and E.J. Pitcher, "As-Built Monte Carlo Model of the Lujan Target System and Comparison of its Neutronic Performance to a Physics Model, LAUR-00-6078 (2000).
[3] J. Knudson, LANSCE-7, private communication (2003).
[4] G.J. Russell, G. Muhrer, E.J. Pitcher, R.A. MacFarlane, and J.J. Jarmer, "Preliminary Comparison Between Calculated Neutron Surface-Flux and Measured Neutron Beam-Flux for the Lujan Upstream/Back-Scattering Supercritical Hydrogen Moderator (Draft) for the proceedings of the 16th Meeting of the International Collaboration on Advanced Neutron Sources, May 12-15, Düsseldorf-Neuss, Germany (2003).
[5] Bicron Corporation, 12345 Kinsman Road, Newbury, OH 44065.
[6] G.F. Knoll, "Radiation Detection and Measurement", 3rd edition, John Wiley & Sons, Inc., p. 548-549 (2000).
[7] J.A. Harvey and N.W. Hill, "Scintillation Detectors for Neutron Physics Research", Nucl. Inst. and Methods, 162, 507 (1979).
[8] S.C. Frankle, R.C. Reedy, and P.G. Young, Evaluated Nuclear Data File B, version VI, National Nuclear Data Center, Brookhaven National Laboratory (2000).
[9] H. Häse, A. Knöpfler, K. Fiederer, U. Schmidt, D. Dubbers, and W. Kaiser, "A long ballistic supermirror guide for cold neutrons at ILL", Nucl. Inst. and Meth., A485, 453 (2002).
[10] D. Dubbers, "The transmission of a lossy curved supermirror neutron guide", Nucl. Inst. and Meth., A349, 302 (1994).
[11] L. Rosta, "Cold neutron research facility at the Budapest Neutron Centre", Appl. Phys. A74, S52 (2002).
[12] Mirrotron LTD., "LANL FP-12 Out of Pile Neutron Guide Section II ER1 and ER2 Section", 1121 Budapest, Konkoly Thege út 29-33, Hungary (2003).